

## Article

# Molecular Interaction and Magnetic Dipole Effects on Fully Developed Nanofluid Flowing via a Vertical Duct Applying Finite Volume Methodology

Kashif Ali <sup>1</sup>, Shabbir Ahmad <sup>2</sup>, Sohail Ahmad <sup>1,3</sup>, Wasim Jamshed <sup>4,\*</sup>, Syed M. Hussain <sup>5</sup>  
and El Sayed M. Tag El Din <sup>6</sup>

- <sup>1</sup> Department of Basic Sciences and Humanities, Muhammad Nawaz Sharif University of Engineering and Technology, Multan 60000, Pakistan
- <sup>2</sup> Institute of Geophysics and Geomatics, China University of Geosciences, Wuhan 430074, China
- <sup>3</sup> Centre for Advanced Studies in Pure and Applied Mathematics, Bahauddin Zakariya University, Multan 60800, Pakistan
- <sup>4</sup> Department of Mathematics, Capital University of Science & Technology, Islamabad 44000, Pakistan
- <sup>5</sup> Department of Mathematics, Faculty of Science, Islamic University of Madinah, Madinah 42351, Saudi Arabia
- <sup>6</sup> Electrical Engineering, Faculty of Engineering and Technology, Future University in Egypt, New Cairo 11835, Egypt
- \* Correspondence: wasiktk@hotmail.com

**Abstract:** Interpreting the complex interaction of nanostructured fluid flow with a dipole in a duct, with peripherally uniform temperature distribution, is the main focus of the current work. This paper also sheds light on the changes in the Nusselt number, temperature profiles, and velocity distributions for the fully developed nanofluid flow in a vertical rectangular duct due to a dipole placed near a corner of the duct. A finite volume approach has been incorporated for the numerical study of the problem. It is interesting to note the unusually lower values of the Nusselt number for the higher values of the ratio  $Gr/Re$ . Due to the nanostructure in the fluid, an enhancement in the Nusselt number has been noted, which is strongly supported by the magnetic field caused by the dipole. However, as the duct shape is transformed from rectangular to square, the Nusselt number is reduced remarkably. Further, as the dipole is brought nearer to the duct corner, the Nusselt number increases significantly. On the other hand, the flow reversal in the middle of the duct has been noted at higher values of the ratio  $Gr/Re$ . The dipole is noted to have a low impact on the reversal flow as well as on the temperature distribution.

**Keywords:** nanofluids; dipole; rectangular duct; mixed convection; laminar flow; finite volume method



**Citation:** Ali, K.; Ahmad, S.; Ahmad, S.; Jamshed, W.; Hussain, S.M.; Tag El Din, E.S.M. Molecular Interaction and Magnetic Dipole Effects on Fully Developed Nanofluid Flowing via a Vertical Duct Applying Finite Volume Methodology. *Symmetry* **2022**, *14*, 2007. <https://doi.org/10.3390/sym14102007>

Academic Editor: Vasilis K. Oikonomou

Received: 19 August 2022

Accepted: 21 September 2022

Published: 25 September 2022

**Publisher's Note:** MDPI stays neutral with regard to jurisdictional claims in published maps and institutional affiliations.



**Copyright:** © 2022 by the authors. Licensee MDPI, Basel, Switzerland. This article is an open access article distributed under the terms and conditions of the Creative Commons Attribution (CC BY) license (<https://creativecommons.org/licenses/by/4.0/>).

## 1. Introduction

Expansion or contraction of the duct has some of the most significant features that are being used in a broad spectrum of industrial and engineering applications, such as power generation systems, heat exchangers, combustion chambers, and electronic equipment. Several authors have conducted extensive analyses of flows and heat transfers in these geometries in previous decades. The majority of these studies are concerned with the control of fluid flow and heat transport. Galanis and Rashidi [1] employed the Graetz problem to find a new solution for an isothermal duct based on hydrodynamically developed convection extended to mass transfer at walls and power-law fluids. Barletta [2] applied the appropriate conditions on a flow that is parallel and onset in the fully formed area of a tilted duct in a circular tube. This research demonstrated how appropriate boundary conditions would help to maintain a parallel flow regime. Umavathi et al. [3] examined free convection nanofluids duct flow and heat transfer through a porous matrix where the fluid flow inside the porous channel was described by the Darcy–Forchheimer–Brinkman

model. A finite-difference approach was chosen to treat the governing model system of equations numerically. It was discovered that the use of nanofluid caused heat transfer enhancement. Cheng et al. [4] analyzed the convective heat transport and buoyancy flow reversal at the entering region of a rectangular duct. Barletta et al. [5,6] had taken the influence of viscous dissipation in a fully developed and slug laminar flow within circular and rectangular ducts by using the Laplace transform technique for finding an analytical solution. Mousavi et al. [7] scrutinized numerically the upshots of a non-uniform magnetization on the biomagnetic fluid flow in a cavity where the magnetic field was induced by a wire having an electric current and suspended outside the cavity. This research explained how much the various magnetic force strengths affected the flow of biomagnetic fluid for different fractions of duct constriction. A numerical analysis was carried out to analyze heat and fluid flow in curvilinear geometries of the duct. Energy and Navier–Stokes equations in the coordinates of curvilinear were solved using the SIMPLEM algorithm by Öztop [8]. Abdellahoum et al. [9] offered a simulation analysis for the turbulent convection in the flow of nanofluids passing through a horizontal duct. A two-dimensional coordinate system was applied to determine the numerical outcomes of the governing system, and simulation was completed for four separate nanofluids (water–CuO, water–Cu, water–Al<sub>2</sub>O<sub>3</sub>, water–Ag) together with pure water. The laminar forced mixed convection, heat transport, and entropy generation in rectangular three-dimensional ducts were explored numerically in [10], where the duct of finite length was heated symmetrically with constant wall temperature. The impacts of buoyancy force, entropy generation, and Magnetohydrodynamic (MHD) mixed convection on nanofluids flow in a duct of an angled step were discussed by Atashafrooz [11]. The results indicated that the Hartmann number has a significant impact on the friction coefficient, Nusselt number, and entropy generation patterns along the lower wall.

Sheikhholeslami [12] used the finite volume method to replicate the entropy generation and water-based nanofluids turbulent flow along a circular duct with twisted-tape turbulators inserted within the pipe. Heat transfer enhancement of nanofluids in a heating system with a helical-twisted-tape turbulator was numerically simulated by using the finite volume approach in [13]. The effects of pitch ratio, width ratio, and Reynolds number on the hydrothermal behavior of nanofluids were shown graphically. The Gaussian elimination method, together with the Galerkin finite element method, have been applied to the computing process for a double diffusion of nanofluid flow into a duct by Hussain et al. [14]. Morini and Spiga [15] suggested an analytical method for studying the transient behavior of a Newtonian fluid in a rectangular duct having natural laminar convection. In this paper, the energy, momentum, and continuity equations were solved by employing a Laplace transform and twofold sine Fourier transform. Selimefendigil and Öztop [16] utilized the finite element method to explore the influences of the double spinning cone system, as well as a magnetic force on mixed convection in some kind of a 3-dimensional porous tube, and the effects of various influencing factors on thermal convection, were also investigated. Ali et al. [17] investigated how the strength of magnetic force influenced the thermal and flow properties of nanofluids within a vertically square duct using both the spectral and finite difference methods. Barletta et al. [18] calculated the free convection and combined force in a rectangular vertical duct with a uniform wall. For each level wall, a different value of heat flux was envisaged, and the energy and momentum equations were iteratively solved by the Galerkin finite element method. Li et al. [19] interpreted the magnetohydrodynamic (MHD) flow of nanofluids across a permeable duct using a mesoscopic method. To depict the Reynolds number effects, Darcy numbers, and the magnetic parameter on the behavior of nanofluids, the lattice Boltzmann method (LBM) was chosen. The work of Ahmad et al. [20] aimed to better understand how a magnetic field in a cavity with dipole interaction affected nanofluid flow. The nanofluid was modeled using a single-phase model, while the system governing the flow model was solved iteratively.

In nature, mixed convection flows, also known as hybrid forced and free convective flows, occur in a variety of technical and industrial applications, such as electronic devices

cooled by fans, solar receivers exposed to air currents, nuclear reactors cooled during an actual emergency, ocean and atmosphere flows, and heat exchangers located in a low-velocity environment. Mixed convection in a nanofluid ( $\text{Al}_2\text{O}_3$ –water) flow, occurring inside a lid-driven quadrilateral cavity under the influence of magnetic force for different conductivity structures by employing the finite element method, has been numerically studied by Selimefendigil and Öztop [21]. Zanchini [22] examined analytically the mixed convection for laminar and steady flow with a thermal viscosity in an annular duct. The findings designated that the cumulative impacts of variable flow rate and buoyancy forces on the averaged friction Fanning factor cross-section significantly affected the flow and that the lower values of such quantities are possible. El. Hasadi et al. [23] scrutinized a laminar mixed convection in a horizontal duct (semicircular) along with the flat wall by employing a finite control volume approach to solve the governing energy and momentum equations numerically. Barletta and Nield [24] analyzed forced mixed convection in a rectangular lid-driven cavity for buoyant laminar flow in view of uniform motion, where the standing sides were heated at various temperatures. Barletta et al. [25] examined a fully developed flow within an axial region having electrical wire immersed in a porous medium. The effects of MHD power, buoyancy, and heat generation were considered due to Joule heating and viscous dissipation. The mixed convection seepage flow was evaluated according to Boussinesq approximation and Darcy law, while the buoyancy effect was modeled by wall temperature. The effect of mixed convection and laminar heat transport enhancement for Lewis number, taking a tube having fixed concentration at the fluid–solid interface and constant heat flux, was discussed by Orfi and Galanis [26]. Barletta [27] analytically investigated mixed convection for a rectangular duct fully developed flow by using Fourier transforms. The temperature field, the velocity field, the friction factor, and the Nusselt number have been evaluated. In a further study of Barletta [28], the Boussinesq approximation was employed to assess the appropriate condition for horizontal mixed convection in a tilted duct and considered a sample case regarding an inclined plane to explain this condition.

Nanofluids are the nanoparticle suspensions in the fluid showing substantial improvement in their properties at modest concentrations of nanoparticles. Many publications regarding nanofluids are about understanding nanofluid behavior, for which direct heat-transfer enhancement plays a pivotal role in many industrial applications, such as transportation, nuclear reactors, electronics, foods, and biomedicines. Geridonmez and Öztop [29] presented a numerical study of nanoparticle flow and heat transport in the duct under the influence of cross differential magnetic fields. The findings were described by the isotherms, streamlines, vorticity contours, and Nusselt number. The thermal conductivity increased due to an increase in the size of the heater or the distinct compositions of nanoparticles. Zhang and Zhang [30] probed the performance of pressure drop and heat transport of magnetic nanofluids with various varying magnetic fields. The outcomes revealed that varying magnetic fields have a stronger effect on local thermal performance than non-magnetic fields. The numerical simulation is discussed in Ref. [31] to address the effects of electric and magnetic fields on nanofluids in a pipe containing titanium–oxide, silicon–oxide, diamond, and copper as nanoparticles and water as the base fluid. Abdelahoum et al. [32] compared various models of viscosity for turbulent nanofluid forced convection ( $\text{Al}_2\text{O}_3$ ) over a thermally driven cavity. Numerical simulations were performed by Zhang and Zhang [33] to study the thermal transmission and magnetic nanofluids' flow properties under magnetic field intensities, magnetic field directions, and volume fractions. According to their findings, the effect of the thermal performance was small in a poor magnetic field but increased significantly in a powerful magnetic field. Ekiciler [34] numerically analyzed flow characteristics and heat transfer by incorporating four dissimilar fluids and modifying the position, length, and altitude of a rib mounted in a two-dimensional channel through turbulent fluid properties and forced convection. Umavathi et al. [35] examined free convection (double diffusive) of nanofluids inside a confined rectangular channel. The equations for momentum and energy were written as difference equations and solved

numerically. The influencing factors of the magnetic field, as well as nanofluid over forced convection flow and thermal irreversibility in a conduit with an immediate contraction, were inspected by Atashafrooz et al. [36]. Mayeli et al. [37] used numerical analysis to interpret the entropy generation and convective heat transfer of the laminar nanofluids' flow across a channel with wavy surfaces under a magnetic field. According to the calculations, skin friction, total entropy generation, and Nusselt number increased as the strength of a magnetic field increased. The micropolar flow within a channel having permeable walls, with the effect of magnetohydrodynamic, was interpreted by Ahmad et al. [38]. Not only skin friction and Nusselt number increased with the effect of the imposed magnetic field but micro-rotational also increased with its effect. To determine the impact of a hybrid methodology on fluid motion and heat transfer, a numerical investigation is carried out by Aidaoui et al. [39]. The authors considered a correlation between multiple promoting approaches to strengthen transfer phenomena in chaotic flow, nanofluid flow, and magnetic induction. The thermal characteristics of copper–water and aluminum oxide–water hybrid nanofluid flow inside a complex non-Darcian porous wavy enclosure was elucidated by Mandal et al. [40]. The left enclosure wall was assumed to be heated and wavy. They noted that the Darcy number caused a reduction in the flow intensity. The same phenomenon was investigated by Biswas et al. [41] and Manna et al. [42], subject to magnetohydrodynamic effects. An analysis of hybrid nanofluid-filled enclosures with thermo-fluidic transport and magnetic field effects was presented by Mondal et al. [43]. Further recent work is elaborated in the refs. [44–46].

This study expresses the novel features of the problem under magnet field effects. For the numerical analysis of the problem, a finite volume technique has been used. The graphical and tabular results describe the dominant effects of the physical parameters on the flow within the duct filled with nanofluids. The presence of a strong magnetic field due to the dipole increases the Nusselt number while the Nusselt number decreases dramatically as the duct shape changes from rectangular to square.

## 2. Governing Equations

The single-phase model (SPM) developed by Xuan and Roetzel [47] has been used to model the nanofluid because the solid's particles are super fine (less than 100 nm) and rapidly fluidized. It may be considered that these particles act somewhat like fluids. Figure 1 describes the location of dipole and geometry of the problem. The nanofluid could be interpreted as a base fluid under the presumptions that there is neither motion slip in between discontinuous phases of both the distributed microscopic particles and the consistent liquid and that there is localized thermal stabilization between the nanostructures and a base fluid. Thus, all energy and motion equations involving pure fluids can be directly applied to nanofluids. However, we have to incorporate the features corresponding to nanofluids while adopting the preexisting dimensionless relation for the base fluids to nanofluids. Therefore, following Xuan and Roetzel [47], the governing equations for the steady, laminar, and incompressible fully developed flow (with Boussinesq hypothesis being used for modeling the buoyancy effect) of a nanofluid in a vertical rectangular duct (with sides  $a$  and  $b$ ), due to an external pressure gradient, may be written as:

$$\frac{\partial u_1}{\partial x_1} + \frac{\partial u_2}{\partial x_2} + \frac{\partial u_3}{\partial x_3} = 0, \quad (1)$$

$$\rho_{nf} \left( u_1 \frac{\partial u_1}{\partial x_1} + u_2 \frac{\partial u_2}{\partial x_2} + u_3 \frac{\partial u_3}{\partial x_3} \right) = -\frac{\partial p}{\partial x_1} + \mu_{nf} \left( \frac{\partial^2 u_1}{\partial x_1^2} + \frac{\partial^2 u_1}{\partial x_2^2} + \frac{\partial^2 u_1}{\partial x_3^2} \right), \quad (2)$$

$$\rho_{nf} \left( u_1 \frac{\partial u_2}{\partial x_1} + u_2 \frac{\partial u_2}{\partial x_2} + u_3 \frac{\partial u_2}{\partial x_3} \right) = -\frac{\partial p}{\partial x_2} + \mu_{nf} \left( \frac{\partial^2 u_2}{\partial x_1^2} + \frac{\partial^2 u_2}{\partial x_2^2} + \frac{\partial^2 u_2}{\partial x_3^2} \right), \quad (3)$$

$$\rho_{nf} \left( u_1 \frac{\partial u_3}{\partial x_1} + u_2 \frac{\partial u_3}{\partial x_2} + u_3 \frac{\partial u_3}{\partial x_3} \right) = -\frac{\partial p}{\partial x_3} + \mu_{nf} \left( \frac{\partial^2 u_3}{\partial x_1^2} + \frac{\partial^2 u_3}{\partial x_2^2} + \frac{\partial^2 u_3}{\partial x_3^2} \right) + (\rho\beta)_{nf} g(T - T_0) + \sigma_{nf} \bar{B}^2 u_3, \quad (4)$$

$$\left( u_1 \frac{\partial T}{\partial x_1} + u_2 \frac{\partial T}{\partial x_2} + u_3 \frac{\partial T}{\partial x_3} \right) = \alpha_{nf} \left( \frac{\partial^2 T}{\partial x_1^2} + \frac{\partial^2 T}{\partial x_2^2} + \frac{\partial^2 T}{\partial x_3^2} \right), \tag{5}$$

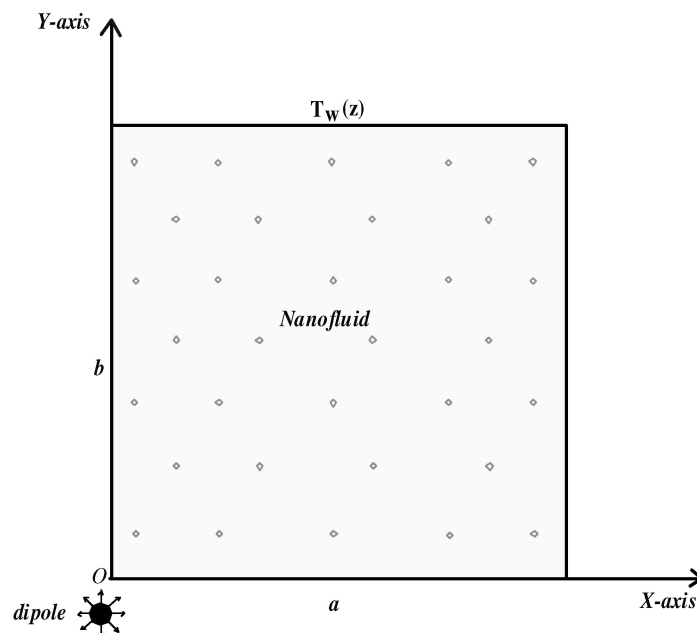


Figure 1. Physical model of the problem.

For the present problem, the velocity field looks like:

$$\vec{V} = (u_1, u_2, u_3) = (0, 0, u_3(x_1, x_2)), \tag{6}$$

where  $x_1$ ,  $x_2$ , and  $x_3$  are the usual three-coordinate directions. It is assumed that the thermal characteristics of fluid, such as dynamic viscosity, thermal conductivity, and thermal diffusivity, do not change. The usual symbols are used for density, thermal diffusivity, temperature, and pressure. Further,  $\sigma_{nf}$  is the electrical diffusivity of the nanofluid, and  $\vec{B} = \bar{\mu}_0 \vec{H}$  is the magnetic field induction with magnetic field intensity  $\vec{H} \left( = \frac{\gamma}{2\pi} \frac{1}{\sqrt{(x_1-x_1^0)^2 + (x_2-x_2^0)^2}} \right)$  situated at  $(x_1^0, x_2^0)$ . Further,  $T_0$  is a reference temperature that describes the relation between local mass density and local temperature. Usually, the reference temperature  $T_0$  is given by:

$$T_0 = \frac{1}{ab} \int_0^b \int_0^a T dx_1 dx_2, \tag{7}$$

This temperature represents the mean flow temperature at a specific cross section of duct. The proposed flow field and the choice  $(0, -\varepsilon_0)$  for the dipole location give rise the system of equations:

$$\frac{\partial u_3}{\partial x_3} = 0, \tag{8}$$

$$\frac{\partial p}{\partial x_1} = \frac{\partial p}{\partial x_2} = 0, \tag{9}$$

$$-\frac{\partial p}{\partial x_3} + \mu_{nf} \left( \frac{\partial^2 u_3}{\partial x_1^2} + \frac{\partial^2 u_3}{\partial x_2^2} \right) + (\rho\beta)_{nf} g(T - T_0) + \sigma_{nf} \bar{\mu}_0^2 \vec{H}^2 u_3 = 0, \tag{10}$$

$$u_3 \frac{\partial T}{\partial x_3} = \alpha_{nf} \left( \frac{\partial^2 T}{\partial x_1^2} + \frac{\partial^2 T}{\partial x_2^2} + \frac{\partial^2 T}{\partial x_3^2} \right), \tag{11}$$

where  $\bar{H}^2 = \left(\frac{\gamma}{2\pi}\right)^2 \left(\frac{1}{x_1^2 + (x_2 + \varepsilon_0)^2}\right)$ . It has been assumed that  $\frac{\partial p}{\partial x_3}$  and  $\frac{\partial T}{\partial x_3}$  is a constant, and pressure is the function of  $x_3$  only with:

$$\frac{\partial T}{\partial x_3} = \frac{dT_w}{dx_3} = \frac{\partial T_0}{\partial x_3} = 4 \frac{\dot{q}_{nf}}{k_{nf}D}, \tag{12}$$

where  $\dot{q}_{nf} = \frac{k_{nf}}{2(a+b)} \left( \int_0^b \left( \frac{\partial T}{\partial x} \Big|_a - \frac{\partial T}{\partial x} \Big|_0 \right) dx_2 + \int_0^a \left( \frac{\partial T}{\partial y} \Big|_b - \frac{\partial T}{\partial y} \Big|_{y=0} \right) dx_1 \right)$  and  $D = \frac{2ab}{a+b}$  are the constant peripherally averaged wall heat flux and the hydraulic diameter of the duct, respectively.

The solution of Equation (11) yields to:

$$u_3 \left( 4 \frac{\dot{q}_{nf}}{k_{nf}D} \right) = \alpha_{nf} \left( \frac{\partial^2 T}{\partial x_1^2} + \frac{\partial^2 T}{\partial x_2^2} \right). \tag{13}$$

Now, we introduce the non-dimensional coordinates as:

$$x = \frac{x_1}{a}, \quad y = \frac{x_2}{a}, \quad \sigma = \frac{b}{a}, \quad \theta = \frac{T - T_w}{T_w - T_0}, \quad \lambda = - \frac{a^2 dp / dx_3}{\mu_f w_0}, \quad w = \frac{u_3}{u_0}, \quad H = \frac{\bar{H}}{H_0}, \quad \varepsilon = \frac{\varepsilon_0}{a} \tag{14}$$

reduce the Equations (10) and (13) to:

$$\lambda + \left( 1 - \phi + \phi \frac{(\rho\beta)_s}{(\rho\beta)_f} \right) (\theta + 1) \left( Gr / Re \right) \left( \frac{1 + \sigma}{2\sigma} \right)^2 + (1 - \phi)^{-2.5} \left( \frac{\partial^2 w}{\partial x^2} + \frac{\partial^2 w}{\partial y^2} \right) - \left\{ 1 + \frac{3 \left( \frac{\sigma_s}{\sigma_f} - 1 \right) \phi}{\left( \frac{\sigma_s}{\sigma_f} + 2 \right) - \left( \frac{\sigma_s}{\sigma_f} - 1 \right) \phi} \right\} MH^2 w = 0, \tag{15}$$

$$\left( \frac{\partial^2}{\partial x^2} + \frac{\partial^2}{\partial y^2} \right) \theta = \frac{(k_s + 2k_f) + \phi(k_f - k_s)}{(k_s + 2k_f) - 2\phi(k_f - k_s)} \left( \frac{1 + \sigma}{\sigma} \right)^2 w. \tag{16}$$

where  $\bar{H}_0 = \frac{\gamma}{2\pi\varepsilon}$  is intensity of magnetic field at origin, which is utilized for the dimensionless magnetic-field strength  $H$ . Additionally,  $\varepsilon = \frac{\varepsilon_0}{a}$  is a concerned dipole location in the non-dimensional XY-coordinate system,  $\sigma = \frac{b}{a}$  is the aspect ratio of the duct, whereas  $\theta$  and  $\lambda$  are, respectively, the dimensionless temperature and pressure gradient.

### 3. Numerical Approach: Finite Volume Method

We note that the governing equation looks like a coupled set of Poisson equations that we want to solve by employing the finite volume method (FVM).

For this, we first present how to discretize a general Poisson equation over a rectangular grid, and then we see what our set of equations looks like when discretized in a similar manner. Around a general grid point “P”, we assume a control volume (CV) of rectangular-shape and integrate the Poisson equation over a domain of this volume, as follows:

$$\nabla^2 u = f \tag{17}$$

$$\iint_{cv} \nabla^2 u dx dy = \iint_{cv} f dx dy \tag{18}$$

$$\int_{y_s}^{y_n} \int_{x_w}^{x_e} \left( \frac{\partial^2 u}{\partial x^2} + \frac{\partial^2 u}{\partial y^2} \right) dx dy = \int_{y_s}^{y_n} \int_{x_w}^{x_e} f dx dy \tag{19}$$

The right-hand side of which is approximated as  $\int_{y_s}^{y_n} \int_{x_w}^{x_e} f dx dy \approx hk f_P$ . Hence,

$$\int_{y_s}^{y_n} \int_{x_w}^{x_e} \left( \frac{\partial^2 u}{\partial x^2} \right) dx dy + \int_{y_s}^{y_n} \int_{x_w}^{x_e} \left( \frac{\partial^2 u}{\partial y^2} \right) dx dy = f_P hk \tag{20}$$

$$\int_{y_s}^{y_n} \left\{ \frac{\partial u}{\partial x} \Big|_{x=x_e} - \frac{\partial u}{\partial x} \Big|_{x=x_w} \right\} dy + \int_{x_w}^{x_e} \left\{ \frac{\partial u}{\partial y} \Big|_{y=y_n} - \frac{\partial u}{\partial y} \Big|_{y=y_s} \right\} dx = f_P hk \tag{21}$$

$$\int_{y_s}^{y_n} \left\{ \frac{u(x_E, y) - u(x_P, y)}{h} - \frac{u(x_P, y) - u(x_W, y)}{k} \right\} dy + \int_{x_w}^{x_e} \left\{ \frac{u(x, y_N) - u(x, y_P)}{h} - \frac{u(x, y_P) - u(x, y_S)}{k} \right\} dx = f_P hk \tag{22}$$

$$\int_{y_s}^{y_n} \left\{ \frac{u(x_E, y) - 2u(x_P, y) + u(x_W, y)}{h} \right\} dy + \int_{x_w}^{x_e} \left\{ \frac{u(x, y_N) - 2u(x, y_P) + u(x, y_S)}{k} \right\} dx = f_P hk \tag{23}$$

$$\left\{ \frac{u(x_E, y_P) - 2u(x_P, y_P) + u(x_W, y_P)}{h} \right\} (y_n - y_s) + \left\{ \frac{u(x_P, y_N) - 2u(x_P, y_P) + u(x_P, y_S)}{k} \right\} (x_e - x_w) = f_P hk \tag{24}$$

$$k \left\{ \frac{u(x_E, y_P) - 2u(x_P, y_P) + u(x_P, y_P)}{h} \right\} + h \left\{ \frac{u(x_P, y_N) - 2u(x_P, y_P) + u(x_P, y_P)}{k} \right\} (x_e - x_w) = f_P hk \tag{25}$$

or

$$k \left\{ \frac{u_E - 2u_P + u_W}{h} \right\} + h \left\{ \frac{u_N - 2u_P + u_S}{k} \right\} = f_P hk \tag{26}$$

Our system of governing equations, when discretized in this way, becomes:

$$\frac{u_E - 2u_P + u_W}{h^2} + \frac{u_S - 2u_P + u_N}{k^2} - \frac{M}{(1-\phi)^{2.5}} H_P^2 u_P = \frac{1}{(1-\phi)^{2.5}} \left\{ 1 - \phi + \phi \frac{(\rho\beta)_s}{(\rho\beta)_f} \right\} (\theta_P + 1) \frac{Gr}{Re} \left( \frac{1+\sigma}{2\sigma} \right)^2 \frac{1}{(1-\phi)^{2.5}} \tag{27}$$

$$\frac{\theta_E - 2\theta_P + \theta_W}{h^2} + \frac{\theta_S - 2\theta_P + \theta_N}{k^2} = \frac{1}{d_2} \left( \frac{1+\delta}{\delta} \right)^2 u_P \tag{28}$$

For solving Equations (15) and (16) when discretized, using Equations (27) and (28), the following appropriate boundary conditions are used:

$$\left. \begin{aligned} w(x_i, y_1) = \theta(x_i, y_1) = w(x_i, y_{n_y}) = \theta(x_i, y_{n_y}) = 0, \\ \forall 1 \leq i \leq n_x \\ w(x_1, y_j) = \theta(x_1, y_j) = w(x_{n_x}, y_j) = \theta(x_{n_x}, y_j) = 0. \\ \forall 1 \leq j \leq n_y \end{aligned} \right\} \tag{29}$$

#### 4. Results and Discussion

We have solved the transformed system of model equations for various values of the governing parameters ( $\lambda$ ,  $\sigma$ ,  $\phi$ , and  $Gr/Re$ , etc.), subject to the boundary conditions, by employing a well-known finite volume method, with the volumetric concentration of

nanoparticles  $\phi$  being the only parameter quantifying the amount of solid particles in the base fluid. Unless otherwise stated, we have taken  $\phi = 0.05$  in the present work.

Physical quantities for the present problem are the Nusselt number  $Nu$  and the Darcy friction factor  $f$ , which are defined as:

$$Nu = \frac{\tilde{q}_w D}{(T_w - T_b) \cdot k_{nf}}, \quad f = \frac{-dp/dz \cdot D}{\rho_{nf} u_0^2 / 2}. \quad (30)$$

In view of Equation (14), we have:

$$Nu = -\frac{k_f (k_s + 2k_f) - 2\phi(k_f - k_s)}{k_{nf} (k_s + 2k_f) + \phi(k_f - k_s)} \cdot \frac{1}{\theta_b}, \quad fRe = 2\lambda \left(1 - \phi + \phi \frac{\rho_s}{\rho_f}\right)^{-1} \cdot \frac{4\sigma^2}{(1 + \sigma)^2}, \quad (31)$$

where

$$\theta_b = \frac{1}{\sigma} \int_{x=0}^1 \int_{y=0}^{\sigma} u(x, y) \theta(x, y) dx dy \quad (32)$$

It is important to mention that  $fRe$  is a prior known constant quantity, which is dependent on the fluid nature, duct shape, and the dimensionless pressure gradient. Therefore, the impact of the governing parameters will only be studied on the Nusselt number  $Nu$  given by Equation (30).

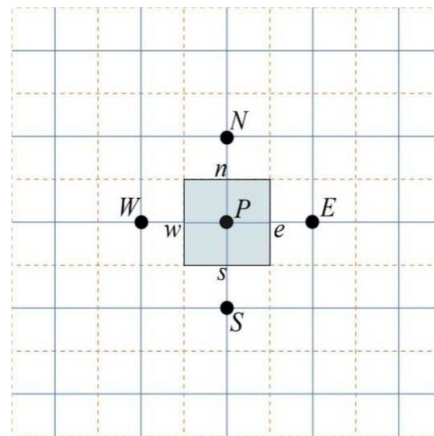
To assess the validity of our numerical solution, we compared our results with those obtained from the spectral method in the limiting case when  $\sigma = 1$ ,  $\lambda = 1$ ,  $\phi = 0.0$ , and  $M = 0$ . For the spectral method, the solution is written in the truncated Fourier series given below:

$$\left. \begin{aligned} u(x, y) &= \sum_{m=1}^{N_1} \sum_{n=1}^{N_2} a_{(m,n)} \sin(m\pi x) \sin(n\pi y) \\ \theta(x, y) &= \sum_{m=1}^{N_1} \sum_{n=1}^{N_2} b_{(m,n)} \sin(m\pi x) \sin(n\pi y) \end{aligned} \right\} \quad (33)$$

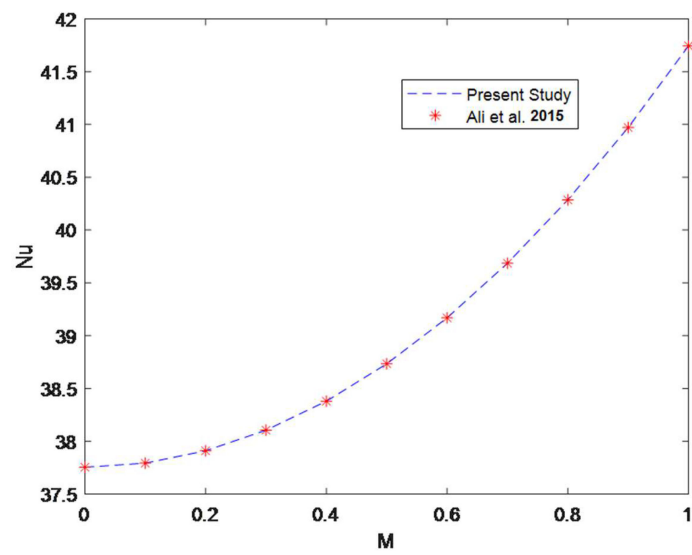
By making use of the orthogonality of basis functions, one arrives at:

$$a_{m,n} = \frac{1}{mn\pi^2} \frac{(1 - (-1)^m)(1 - (-1)^n)}{\left\{ \frac{(Gr/Re)}{4\pi^2(m^2+n^2)} + 0.25\pi^2(m^2+n^2) \right\}}, \quad b_{m,n} = \frac{a_{m,n}}{\pi^2(m^2+n^2)} \quad (34)$$

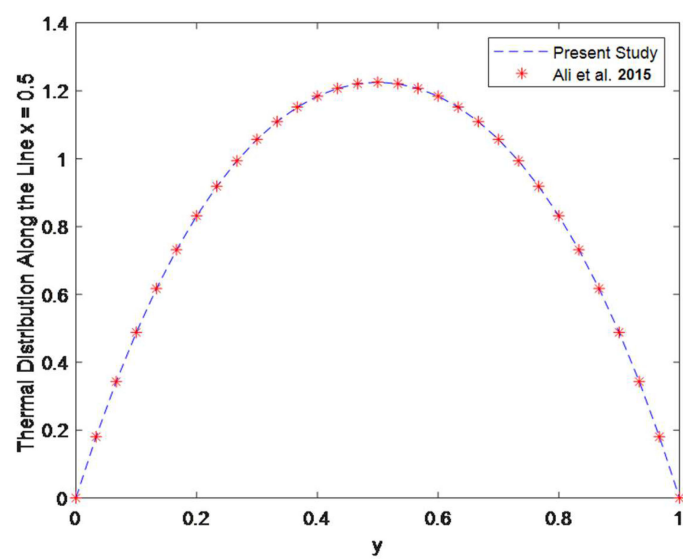
An excellent comparison of our numerical results with the Spectral method (given in Table 1) provides a source of validation for our computational technique. In order to present rigorous and detailed validity of our computer code, we compare (in Figure 2b–d) our numerical results with the existing scientific literature (Ali et al. [17]) for the special case of pressure-gradient driven flow in the square duct without any nearby laying dipole. Excellent comparison of our heat transfer results with the related problem (Ali et al. [17]) is a source of satisfaction for the authors. On the other hand, Table 2 shows the thermo-physical properties of the base fluid (water) and the solid particles (silver).



(a)



(b)



(c)

Figure 2. Cont.

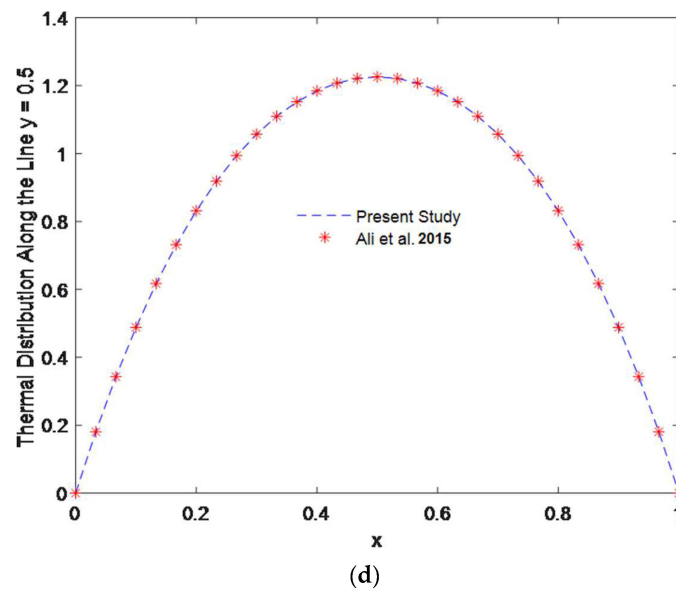


**Figure 2.** (a) Control volume domain at a specific mesh point P. (b) Comparison of our numerical results for the Nusselt number  $Nu$  with literature Ali et al. [17], for the limiting case. (c) Comparison of our numerical results along the line  $x = 0.5$  with the literature Ali et al. [17], for the limiting case. (d) Comparison of our numerical results along the line  $y = 0.5$  with the literature Ali et al. [17], for the limiting case.

**Table 1.** Comparison of present results for  $Nu$  in the limiting case when  $\sigma = 1$ ,  $\lambda = 1$ ,  $\phi = 0.0$ , and  $M = 0$ .

$Gr/Re$	$Nu$ (Present Method)	$Nu$ (Spectral Method)
1	$1.1746 \times 10^4$	$1.1745 \times 10^4$
10	$1.2292 \times 10^4$	$1.2291 \times 10^4$
100	$1.8436 \times 10^4$	$1.8433 \times 10^4$
1000	$1.4612 \times 10^4$	$1.4608 \times 10^4$
5000	$1.9351 \times 10^4$	$1.9343 \times 10^4$

**Table 2.** Thermo-physical properties of nanoparticles and water.

Thermo-Physical	$\rho$ ( $\text{kgm}^{-3}$ )	$C_p$ ( $\text{Jkg}^{-1}\text{K}^{-1}$ )	$k$ ( $\text{Wm}^{-1}\text{K}^{-1}$ )	$\beta$ ( $\text{K}^{-1}$ )
Water ( $\text{H}_2\text{O}$ )	997.1	4179	0.613	$21 \times 10^{-5}$
Silver (Ag)	10500	235	429	$1.89 \times 10^{-5}$

Moreover, it is interesting to note (from Table 1) the unusually higher values of the Nusselt number  $Nu$  for the higher  $Gr/Re$  ratio. As the ratio is increased, the velocity distribution is significantly lowered (as predicted in the next section). As a result, Equation (13) becomes very similar to a Laplace equation with Dirichlet boundary conditions (the function to be found is zero on the boundary), which gives the numerical solution almost coincident to the  $XY$ -plane. Consequently, the Nusselt number, being the reciprocal of a double integral of dimensionless temperature, becomes very large. In Table 3, we observe the impact of the magnetic parameter  $M$  and the aspect ratio  $\sigma$  on the Nusselt number  $Nu$ , for the particular case of forced convection, that is,  $Gr/Re = 0$ .

**Table 3.** Nusselt number variation with  $\sigma$  and  $M$  for the fixed  $\lambda = 200$ ,  $\frac{Gr}{Re=0}$ ,  $\phi = 0.02$ , and  $\varepsilon = 0.2$ .

$\sigma$	$Nu$				
	$M = 0$	$M = 50$	$M = 100$	$M = 150$	$M = 200$
0.2	18.7016	19.8204	20.9379	22.0550	23.1728
0.4	1.2432	1.4441	1.6535	1.8710	2.0967
0.6	0.3056	0.3824	0.4654	0.5546	0.6497
0.8	0.1342	0.1753	0.2207	0.2701	0.3235
1.0	0.0808	0.1073	0.1367	0.1688	0.2037

A significant rise in  $Nu$  is noted due to a strong magnetic field. However, as the duct shape is transformed from rectangular to square form, the Nusselt number is reduced remarkably. For the mixed convection scenario, the physical quantities of interest (that is,  $Nu$ ) is given in Table 4.

**Table 4.** Variation in  $Nu$  with  $\sigma$  and  $M$  for the fixed  $\lambda = 200$ ,  $Gr/Re = 100$ ,  $\phi = 0.02$ , and  $\varepsilon = 0.2$ .

$\sigma$	$Nu$				
	$M = 0$	$M = 50$	$M = 100$	$M = 150$	$M = 200$
0.2	1.2608	1.3143	1.3677	1.4208	1.4737
0.4	0.5254	0.5767	0.6289	0.6819	0.7359
0.6	0.2800	0.3181	0.3576	0.3984	0.4406
0.8	0.1804	0.2088	0.2384	0.2693	0.3014
1.0	0.1318	0.1537	0.1766	0.2005	0.2254

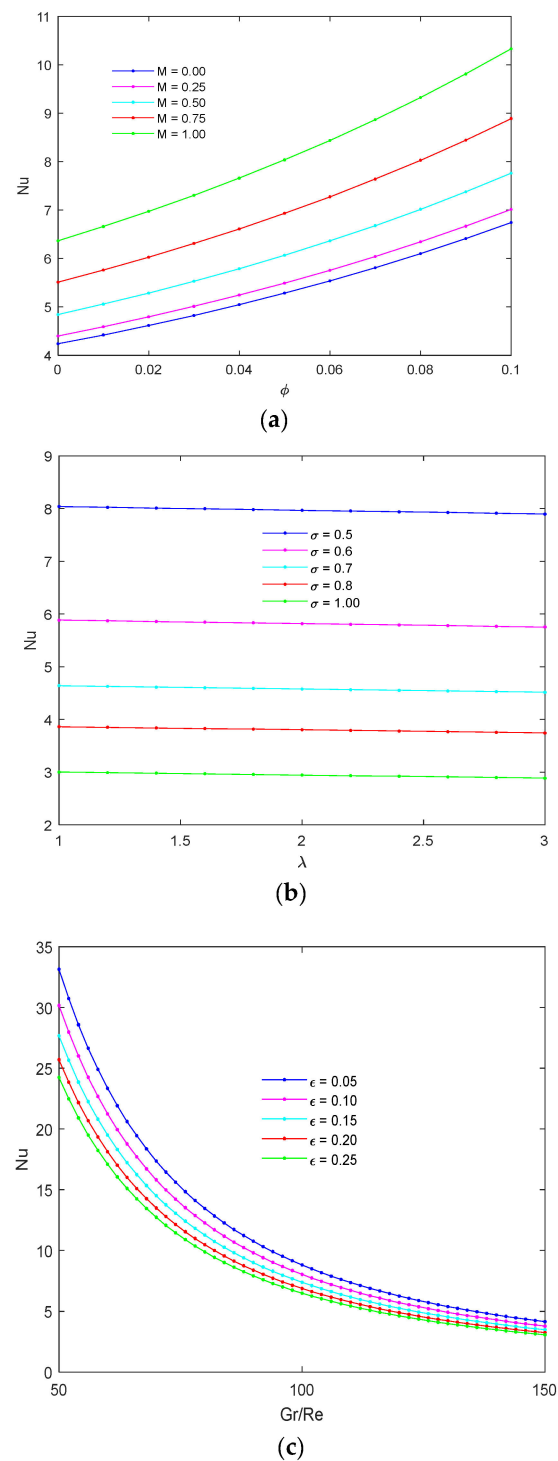
It is noted that the forced convection is far more effective quantitatively on a rectangular duct.

An analysis of  $Nu$  against both the ratios of  $Gr/Re$  (negative and positive) is provided in Table 5. Some more discussion is required to interpret the case for which both  $Gr$  and  $Re$  are less than zero. A cautious examination is essential in subsequent studies to further investigate the stability of the laminar temperature as well as velocity distributions, which is out of the aims of the current work.

**Table 5.** Variation in  $Nu$  with  $Gr/Re$  and  $M$  for the fixed  $\lambda = 200$ ,  $\sigma = 0.5$ ,  $\phi = 0.02$ , and  $\varepsilon = 0.2$ .

$Gr/Re$	$Nu$				
	$M = 0$	$M = 50$	$M = 100$	$M = 150$	$M = 200$
−100	2.3919	4.6080	7.4516	10.8838	14.8753
−50	1.1507	1.5449	1.9836	2.4648	2.9868
0	0.5583	0.6756	0.8004	0.9325	1.0717
50	0.4289	0.4940	0.5619	0.6323	0.7053
100	0.3729	0.4173	0.4630	0.5099	0.5581

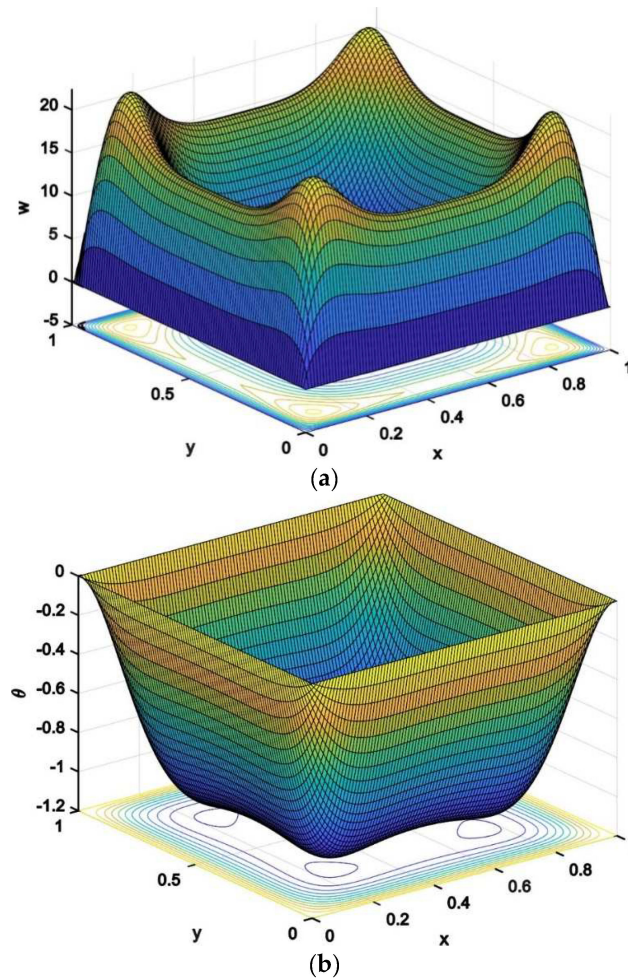
Further, Figure 3a,b are referred in order to obtain a further insight into the dependence of the Nusselt number  $Nu$  on different governing parameters. Obviously, there is a significant increase in  $Nu$  irrespective of the strength of the magnetic field produced by the dipole (please see Figure 3a).



**Figure 3.** (a) Variation in the Nusselt number with different  $\phi$  and  $M$ . (b) Variation in the Nusselt number with different  $\lambda$  and  $\sigma$ . (c) Variation in the Nusselt number with different ratio  $\frac{Gr}{Re}$  and  $\epsilon$ .

Figure 4a,b give the distribution of dimensionless velocity and temperature distributions across the square duct, in the absence of any magnetic effects. The non-dimensional pressure gradient  $\lambda$  is negative in the present case, which implies the existence of an upward deriving force acting on the fluid. However, the ratio  $\frac{Gr}{Re}$  causes a downward force in the middle of the duct (the force is not very influential near the duct walls due to the no-slip boundary condition). An obvious point of concern is to check the possibility of flow reversal, which can happen at the points where the velocity is negative and that cannot be

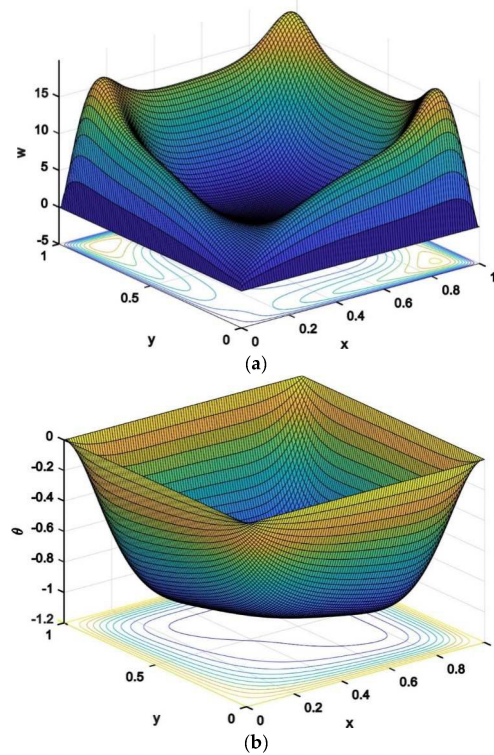
explicitly known from the above figures. We, therefore, focus our attention on the velocity cross-section in the middle of the duct.



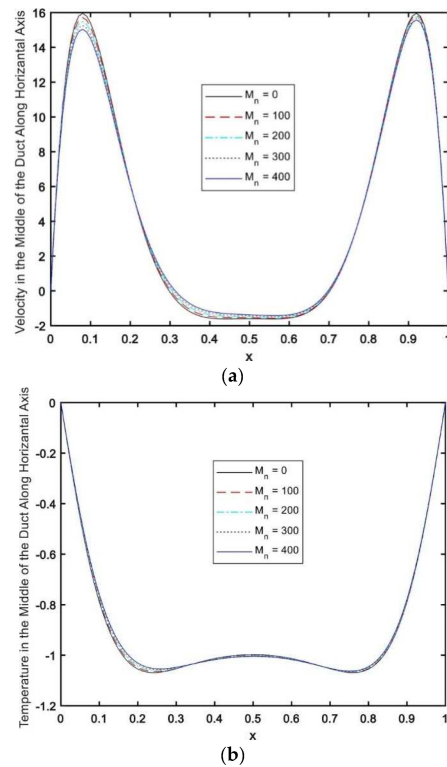
**Figure 4.** (a) Velocity distribution in the duct for the fixed  $M = 0$ ,  $Gr/Re = 10^4$ ,  $\sigma = 1$ ,  $\phi = 0.02$ ,  $\varepsilon = 0.2$ , and  $\lambda = 10$  (b) Temperature distribution in the duct for the fixed  $M = 0$ ,  $Gr/Re = 10^4$ ,  $\sigma = 1$ ,  $\phi = 0.02$ ,  $\varepsilon_0 = 0.2$ , and  $\lambda = 10$ .

Figure 5a,b are portrayed to see how the dipole located at  $(0, -\varepsilon_0)$  affects the velocity and temperature distributions. An obvious impact is the distortion of symmetry of the profiles. Further, as obvious from the governing equations, the intensity with which the temperature and velocity distributions are affected, at a certain point in the flow field, depends upon its distance from the dipole. We confirm this format.

Flow reversal in the middle of the duct is significant at higher values of the ratio  $Gr/Re$ , from Figure 6a. Further, the dipole is noted to have a low impact on the reversal flow as well as on the temperature distribution (Figure 6b). It can thus be inferred that the dipole affects the velocity and temperature distributions on the duct corner that is nearest to the dipole.



**Figure 5.** (a) Velocity distribution in the duct for the fixed  $M = 100$ ,  $Gr/Re = 10^4$ ,  $\sigma = 1$ ,  $\phi = 0.02$ ,  $\epsilon = 0.2$ , and  $\lambda = 10$ . (b) Temperature distribution in the duct for the fixed  $M = 100$ ,  $Gr/Re = 10^4$ ,  $\sigma = 1$ ,  $\phi = 0.02$ ,  $\epsilon = 0.2$ , and  $\lambda = 10$ .



**Figure 6.** (a) Velocity distribution in the duct for the fixed  $Gr/Re = 10^4$ ,  $\sigma = 1$ ,  $\phi = 0.02$ ,  $\epsilon = 0.2$ , and  $\lambda = 10$ . (b) Temperature distribution in the duct for the fixed  $Gr/Re = 10^4$ ,  $\sigma = 1$ ,  $\phi = 0.02$ ,  $\epsilon = 0.2$ , and  $\lambda = 10$ .

## 5. Conclusions

The purpose of the paper is to study how the Nusselt number, temperature profiles, and velocity distributions for the fully developed nanofluid flow in a vertical rectangular duct are affected by the magnetic field produced by a nearby placed dipole. Governing equations are discretized using a finite volume approach, and the algebraic system thus obtained is iteratively solved. The computational technique is rigorously validated by comparing our numerical results with the existing scientific literature for a limiting case of pressure-gradient-driven flow in the square duct in the absence of any dipole.

It is noted that the quantity  $fRe$  is a prior known constant quantity, which is dependent on the fluid nature, duct shape, and the dimensionless pressure gradient. Therefore, the impact of the governing parameters has been studied on the Nusselt number only.

As the duct shape is transformed from rectangular to square, we notice more than 200% reduction in the Nusselt number, even in the presence of a very strong magnetic field. As the ratio  $(Gr/Re)$  is increased, the velocity distribution is reduced to such an extent that even flow reversal is predicted to occur in the middle of the duct. Finally, the temperature distribution and the flow reversal are not significantly affected by the dipole.

The finite volume method could be applied to a variety of physical and technical challenges in the future [48–55]. Some recent developments exploring the significance of the considered research domain are reported in the studies [56–65].

**Author Contributions:** Conceptualization, K.A. and S.A. (Shabbir Ahmad); methodology, K.A.; software, S.A. (Sohail Ahmad); validation, W.J., K.A. and S.M.H.; formal analysis, S.A. (Sohail Ahmad); investigation, E.S.M.T.E.D.; resources, S.M.H.; data curation, S.A. (Shabbir Ahmad); writing—original draft preparation, S.A. (Shabbir Ahmad); writing—review and editing, S.A. (Sohail Ahmad); visualization, W.J.; supervision, K.A.; project administration, E.S.M.T.E.D.; funding acquisition, E.S.M.T.E.D. All authors have read and agreed to the published version of the manuscript.

**Funding:** This research received no external funding.

**Data Availability Statement:** Data will be provided by the authors on request.

**Acknowledgments:** Authors are grateful to the Deanship of Scientific Research, Islamic University of Madinah, Ministry of Education, KSA for supporting this research work through research project grant under Research Group Program/1/804.

**Conflicts of Interest:** The authors declare no conflict of interest.

## Nomenclature

### List of symbols

$H$	magnetic field
$\bar{H}$	magnetic field intensity
$H$	magnetic field strength [T]
$\bar{B}$	magnetic field induction
$\bar{H}_0$	magnetic field intensity at the origin
$x_E$	ordinate of eastward located neighboring point of point P
$x_P$	ordinate of general point P
$x_W$	ordinate of westward located neighboring point of point P
$x_N$	ordinate of northward located neighboring point of point P
$u_E$	velocity at the eastward located point E
$u_P$	velocity of general point P
$u_W$	velocity at the westward located point W
$u_N$	velocity at the northward located point N
$y_P$	abscissa of general point P
$y_S$	abscissa of the ordinate of southward located neighboring point of point P
$y_N$	abscissa of the ordinate of northward located neighboring point of point P

$k$	grid space along vertical direction
$h$	grid space along horizontal direction
$f_P$	value of the function at point
$a_{n,m}$	coefficient for the spectral expression for u
$b_{n,m}$	coefficient for the spectral expression for u
$M$	magnetic parameter
$N_u$	Nusselt number
$Re$	Reynolds number
$T$	temperature [K]
$T_0$	reference temperature
$D$	hydraulic diameter of the duct
$\dot{q}_{mf}$	constant peripherally averaged wall heat flux
Greek letters	
$\theta$	dimensionless temperature
$\phi$	nanoparticle volume fraction
$\rho$	density [ $kg.m^{-3}$ ]
$\rho_s$	density for the solid particles
$\rho_f$	density of the base fluids
$\rho_{nf}$	density of the nanofluids
$\sigma_{nf}$	electrical diffusivity of the nanofluid
$\varepsilon$	corresponding location of the dipole
$\sigma$	aspect ratio of the duct
$\lambda$	pressure gradient

## References

1. Galanis, N.; Rashidi, M. Entropy generation in non-Newtonian fluids due to heat and mass transfer in the entrance region of ducts. *Heat Mass Transf.* **2012**, *48*, 1647–1662. [[CrossRef](#)]
2. Barletta, A. Parallel and non-parallel laminar mixed convection flow in an inclined tube: The effect of the boundary conditions. *Int. J. Heat Fluid Flow* **2008**, *29*, 83–93. [[CrossRef](#)]
3. Umavathi, J.C.; Ojjela, O.; Vajravelu, K. Numerical analysis of natural convective flow and heat transfer of nanofluids in a vertical rectangular duct using Darcy-Forchheimer-Brinkman model. *Int. J. Therm. Sci.* **2017**, *111*, 511–524. [[CrossRef](#)]
4. Cheng, C.H.; Weng, C.J.; Aung, W. Buoyancy-assisted flow reversal and convective heat transfer in entrance region of a vertical rectangular duct. *Int. J. Heat Fluid Flow* **2000**, *21*, 403–411. [[CrossRef](#)]
5. Barletta, A.; Magyari, E. Forced convection with viscous dissipation in the thermal entrance region of a circular duct with prescribed wall heat flux. *Int. J. Heat Mass Transf.* **2007**, *50*, 26–35. [[CrossRef](#)]
6. Barletta, A.; Pulvirenti, B. Forced convection with slug flow and viscous dissipation in a rectangular duct. *Int. J. Heat Mass Transf.* **2000**, *43*, 725–740. [[CrossRef](#)]
7. Mousavi, S.M.; Darzi, A.A.R.; Akbari, O.A.; Toghraie, D.; Marzban, A. Numerical study of biomagnetic fluid flow in a duct with a constriction affected by a magnetic field. *J. Magn. Magn. Mater.* **2019**, *473*, 42–50. [[CrossRef](#)]
8. Öztop, H.F. Numerical study of flow and heat transfer in curvilinear ducts: Applications of elliptic grid generation. *Appl. Math. Comput.* **2005**, *168*, 1449–1460. [[CrossRef](#)]
9. Abdellahoum, C.; Mataoui, A.; Öztop, H.F. Turbulent forced convection of nanofluid over a heated shallow cavity in a duct. *Powder Technol.* **2015**, *277*, 126–134. [[CrossRef](#)]
10. Yang, G.; Wu, J.; Yan, L. Flow reversal and entropy generation due to buoyancy assisted mixed convection in the entrance region of a three dimensional vertical rectangular duct. *Int. J. Heat Mass Transf.* **2013**, *67*, 741–751. [[CrossRef](#)]
11. Atashafrooz, M. The effects of buoyancy force on mixed convection heat transfer of MHD nanofluid flow and entropy generation in an inclined duct with separation considering Brownian motion effects. *J. Therm. Anal. Calorim.* **2019**, *138*, 3109–3126. [[CrossRef](#)]
12. Sheikholeslami, M.; Jafaryar, M.; Li, Z. Second law analysis for nanofluid turbulent flow inside a circular duct in presence of twisted tape turbulators. *J. Mol. Liq.* **2018**, *263*, 489–500. [[CrossRef](#)]
13. Sheikholeslami, M.; Jafaryar, M.; Li, Z. Nanofluid turbulent convective flow in a circular duct with helical turbulators considering CuO nanoparticles. *Int. J. Heat Mass Transf.* **2018**, *124*, 980–989. [[CrossRef](#)]
14. Hussain, S.; Öztop, H.F.; Jamal, M.; Hamdeh, N.A. Double diffusive nanofluid flow in a duct with cavity heated from below. *Int. J. Mech. Sci.* **2017**, *131*, 535–545. [[CrossRef](#)]
15. Morini, G.; Spiga, M. Transient laminar natural convection along rectangular ducts. *Int. J. Heat Mass Transfer.* **2001**, *44*, 4703–4710. [[CrossRef](#)]
16. Selimefendigil, F.; Öztop, H.F. Combined effects of double rotating cones and magnetic field on the mixed convection of nanofluid in a porous 3D U-bend. *Int. Commun. Heat Mass Transf.* **2020**, *116*, 104703. [[CrossRef](#)]

17. Ali, K.; Ahmad, S.; Ahmad, S.; Ashraf, M.; Asif, M. On the interaction between the external magnetic field and nanofluid inside a vertical square duct. *AIP Adv.* **2015**, *5*, 107120. [[CrossRef](#)]
18. Barletta, A.; di Schio, E.R.; Zanchini, E. Combined forced and free flow in a vertical rectangular duct with prescribed wall heat flux. *Int. J. Heat Fluid Flow* **2003**, *24*, 874–887. [[CrossRef](#)]
19. Li, Z.; Sheikholeslami, M.; Mittal, A.S.; Shafee, A.; Haq, R.U. Nanofluid heat transfer in a porous duct in the presence of Lorentz forces using the lattice Boltzmann method. *Eur. Phys. J. Plus* **2019**, *134*, 30. [[CrossRef](#)]
20. Ahmad, S.; Cai, J.; Ali, K. Prediction of new vortices in single-phase nanofluid due to dipole interaction. *J. Therm. Anal. Calorim.* **2022**, *147*, 461–475. [[CrossRef](#)]
21. Selimefendigil, F.; Öztop, H.F. Modeling and optimization of MHD mixed convection in a lid-driven trapezoidal cavity filled with alumina–water nanofluid: Effects of electrical conductivity models. *Int. J. Mech. Sci.* **2018**, *136*, 264–278. [[CrossRef](#)]
22. Zanchini, E. Mixed convection with variable viscosity in a vertical annulus with uniform wall temperatures. *Int. J. Heat Mass Transf.* **2008**, *51*, 30–40. [[CrossRef](#)]
23. el Hasadi, Y.M.F.; Busedra, A.A.; Rustum, I.M. Laminar mixed convection in the entrance region of horizontal semicircular ducts with the flat wall at the top. *J. Heat Transf.* **2007**, *129*, 1203–1211. [[CrossRef](#)]
24. Barletta, A.; Nield, D. Mixed convection with viscous dissipation and pressure work in a lid-driven square enclosure. *Int. J. Heat Mass Transf.* **2009**, *52*, 4244–4253. [[CrossRef](#)]
25. Barletta, A.; Magyari, E.; Lazzari, S.; Pop, I. Mixed convection with heating effects in a vertical porous annulus with a radially varying magnetic field. *Int. J. Heat Mass Transf.* **2008**, *51*, 5777–5784. [[CrossRef](#)]
26. Orfi, J.; Galanis, N. Mixed convection with heat and mass transfer in horizontal tubes. *Int. Commun. Heat Mass Transf.* **2005**, *32*, 511–519. [[CrossRef](#)]
27. Barletta, A. Fully developed mixed convection and flow reversal in a vertical rectangular duct with uniform wall heat flux. *Int. J. Heat Mass Transf.* **2002**, *45*, 641–654. [[CrossRef](#)]
28. Barletta, A. On the existence of parallel flow for mixed convection in an inclined duct. *Int. J. Heat Mass Transf.* **2005**, *48*, 2042–2049. [[CrossRef](#)]
29. Geridonmez, B.P.; Öztop, H. MHD natural convection in a cavity in the presence of cross partial magnetic fields and Al<sub>2</sub>O<sub>3</sub>–water nanofluid. *Comput. Math. Appl.* **2020**, *80*, 2796–2810. [[CrossRef](#)]
30. Zhang, X.; Zhang, Y. Experimental study on enhanced heat transfer and flow performance of magnetic nanofluids under alternating magnetic field. *Int. J. Therm. Sci.* **2021**, *164*, 106897. [[CrossRef](#)]
31. Umavathi, J.; Öztop, H.F. Investigation of MHD and applied electric field effects in a conduit cramed with nanofluids. *Int. Commun. Heat Mass Transf.* **2021**, *121*, 105097. [[CrossRef](#)]
32. Abdellahoum, C.; Mataoui, A.; Öztop, H.F. Comparison of viscosity variation formulations for turbulent flow of Al<sub>2</sub>O<sub>3</sub>–water nanofluid over a heated cavity in a duct. *Adv. Powder Technol.* **2015**, *26*, 1210–1218. [[CrossRef](#)]
33. Zhang, X.; Zhang, Y. Heat transfer and flow characteristics of Fe<sub>3</sub>O<sub>4</sub>–water nanofluids under magnetic excitation. *Int. J. Therm. Sci.* **2021**, *163*, 106826. [[CrossRef](#)]
34. Ekiciler, R. Effects of novel hybrid nanofluid (TiO<sub>2</sub>–Cu/EG) and geometrical parameters of triangular rib mounted in a duct on heat transfer and flow characteristics. *J. Therm. Anal. Calorim.* **2021**, *143*, 1371–1387. [[CrossRef](#)]
35. Umavathi, J.; Buonomo, B.; Manca, O.; Shereme, M. Double diffusion in a rectangular duct using metals or oxides suspended in a viscous fluid. *Therm. Sci. Eng. Prog.* **2021**, *21*, 100793. [[CrossRef](#)]
36. Atashafrooz, M.; Sheikholeslami, M.; Sajjadi, H.; Delouei, A.A. Interaction effects of an inclined magnetic field and nanofluid on forced convection heat transfer and flow irreversibility in a duct with an abrupt contraction. *J. Magn. Magn. Mater.* **2019**, *478*, 216–226. [[CrossRef](#)]
37. Mayeli, P.; Hesami, H.; Moghaddam, M.H.D.F. Numerical investigation of the MHD forced convection and entropy generation in a straight duct with sinusoidal walls containing water–Al<sub>2</sub>O<sub>3</sub> nanofluid. *Numer. Heat Transf. Part A Appl.* **2017**, *71*, 1235–1250. [[CrossRef](#)]
38. Ahmad, S.; Ali, K.; Ahmad, S.; Cai, J. Numerical Study of Lorentz Force Interaction with Micro Structure in Channel Flow. *Energies* **2021**, *14*, 4286. [[CrossRef](#)]
39. Aidaoui, L.; Lasbet, Y.; Selimefendigil, F. Improvement of transfer phenomena rates in open chaotic flow of nanofluid under the effect of magnetic field: Application of a combined method. *Int. J. Mech. Sci.* **2020**, *179*, 105649. [[CrossRef](#)]
40. Mandal, D.K.; Biswas, N.; Manna, N.K.; Gorla, R.S.R.; Chamkha, A.J. Magneto-hydrothermal performance of hybrid nanofluid flow through a non-Darcian porous complex wavy enclosure. *Eur. Phys. J. Plus* **2022**, *231*, 2695–2712. [[CrossRef](#)]
41. Biswas, N.; Mondal, M.K.; Mandal, D.K.; Manna, N.K.; Gorla, R.S.R.; Chamkha, A.J. A narrative loom of hybrid nanofluid-filled wavy walled tilted porous enclosure imposing a partially active magnetic field. *Int. J. Mech. Sci.* **2022**, *217*, 107028. [[CrossRef](#)]
42. Manna, N.K.; Mondal, M.K.; Biswas, N. A novel multi-banding application of magnetic field to convective transport system filled with porous medium and hybrid nanofluid. *Phys. Scr.* **2021**, *96*, 065001. [[CrossRef](#)]
43. Mondal, M.K.; Biswas, N.; Datta, A.; Mandal, D.K.; Manna, N.K. Thermofluidic transport phenomena of hybrid nanofluid in a porous wavy enclosure imposing magnetic fields. *Mater. Today Proc.* **2022**, *52*, 505–512. [[CrossRef](#)]
44. Afridi, M.I.; Ashraf, M.U.; Qasim, M.; Wakif, A. Numerical simulation of entropy transport in the oscillating fluid flow with transpiration and internal fluid heating by GGDQM. *Waves Random Complex Media* **2022**, 1–19. [[CrossRef](#)]

45. Afridi, M.I.; Qasim, M.; Khan, N.A.; Makinde, O.D. Minimization of Entropy Generation in MHD Mixed Convection Flow with Energy Dissipation and Joule Heating: Utilization of Sparrow-Quack-Boerner Local Non-Similarity Method. *Defect Diffus. Forum* **2018**, *387*, 63–77. [[CrossRef](#)]
46. Afridi, M.I.; Muhammad, I.; Qasim, M.; Shafie, S.; Makinde, O.D. Entropy generation analysis of spherical and non-spherical Ag-Water nanofluids in a porous medium with magnetic and porous dissipation. *J. Nanofluids* **2018**, *7*, 951–960. [[CrossRef](#)]
47. Xuan, Y.; Roetzel, W. Conceptions for heat transfer correlation of nanofluids. *Int. J. Heat Mass Transf.* **2000**, *43*, 3701–3707. [[CrossRef](#)]
48. Ali, K.; Ahmad, S.; Baluch, O.; Jamshed, W.; Mohamed, R.; Eid, M.R.; Pasha, A.A. Numerical study of magnetic field interaction with fully developed flow in a vertical duct. *Alex. Eng. J.* **2022**, *61*, 11351–11363. [[CrossRef](#)]
49. Jamshed, W.; Aziz, A. Entropy Analysis of TiO<sub>2</sub>-Cu/EG Casson Hybrid Nanofluid via Cattaneo-Christov Heat Flux Model. *Appl. Nanosci.* **2018**, *8*, 1–14.
50. Rasool, G.; Saeed, A.M.; Lare, A.I.; Abderrahmane, A.; Guedri, K.; Vaidya, H. Darcy-Forchheimer Flow of Water Conveying Multi-Walled Carbon Nanoparticles through a Vertical Cleveland Z-Staggered Cavity Subject to Entropy Generation. *Micromachines* **2022**, *13*, 744. [[CrossRef](#)]
51. Shafiq, A.; Mebarek-Oudina, F.; Sindhu, T.N.; Rasool, G. Sensitivity analysis for Walters-B nanoliquid flow over a radiative Riga surface by RSM. *Sci. Iran.* **2022**, *29*, 1236–1249.
52. Batool, S.; Rasool, G.; Alshammari, N.; Khan, I.; Kaneez, H.; Hamadneh, N. Numerical analysis of heat and mass transfer in micropolar nanofluids flow through lid driven cavity: Finite volume approach. *Case Stud. Therm. Eng.* **2022**, *37*, 102233. [[CrossRef](#)]
53. Rasool, G.; Shafiq, A.; Alqarni, M.S.; Wakif, A.; Khan, I.; Bhutta, M.S. Numerical Scrutinization of Darcy-Forchheimer Relation in Convective Magnetohydrodynamic Nanofluid Flow Bounded by Nonlinear Stretching Surface in the Perspective of Heat and Mass Transfer. *Micromachines* **2021**, *12*, 374. [[CrossRef](#)] [[PubMed](#)]
54. Jamshed, W.; Nisar, K.S. Computational single phase comparative study of Williamson nanofluid in parabolic trough solar collector via Keller box method. *Int. J. Energy Res.* **2021**, *45*, 10696–10718. [[CrossRef](#)]
55. Jamshed, W.; Devi, S.U.; Nisar, K.S. Single phase-based study of Ag-Cu/EO Williamson hybrid nanofluid flow over a stretching surface with shape factor. *Phys. Scr.* **2021**, *96*, 065202. [[CrossRef](#)]
56. Jamshed, W.; Nisar, K.S.; Ibrahim, R.W.; Shahzad, F.; Eid, M.R. Thermal expansion optimization in solar aircraft using tangent hyperbolic hybrid nanofluid: A solar thermal application. *J. Mater. Res. Technol.* **2021**, *14*, 985–1006. [[CrossRef](#)]
57. Jamshed, W.; Nisar, K.S.; Ibrahim, R.W.; Mukhtar, T.; Vijayakumar, V.; Ahmad, F. Computational frame work of Cattaneo-Christov heat flux effects on Engine Oil based Williamson hybrid nanofluids: A thermal case study. *Case Stud. Therm. Eng.* **2021**, *26*, 101179. [[CrossRef](#)]
58. Rasool, G.; Shafiq, A.; Hussain, S.; Zaydan, M.; Wakif, A.; Chamkha, A.J.; Bhutta, M.S. Significance of Rosseland's Radiative Process on Reactive Maxwell Nanofluid Flows over an Isothermally Heated Stretching Sheet in the Presence of Darcy-Forchheimer and Lorentz Forces: Towards a New Perspective on Buongiorno's Model. *Micromachines* **2022**, *13*, 368. [[CrossRef](#)]
59. Pasha, A.; Islam, N.; Jamshed, W.; Alam, M.I.; Jameel, A.G.A.; Juhany, K.A.; Alsulami, R. Statistical analysis of viscous hybridized nanofluid flowing via Galerkin finite element technique. *Int. Commun. Heat Mass Transf.* **2022**, *137*, 106244. [[CrossRef](#)]
60. Zari, I.; Shafiq, A.; Rasool, G.; Sindhu, T.N.; Khan, T.S. Double-stratified Marangoni boundary layer flow of Casson nanoliquid: Probable error application. *J. Thermal Anal. Calorim.* **2022**, *147*, 6913–6929. [[CrossRef](#)]
61. Hussain, S.M.; Jamshed, W.; Pasha, A.A.; Adil, M.; Akram, M. Galerkin finite element solution for electromagnetic radiative impact on viscid Williamson two-phase nanofluid flow via extendable surface. *Int. Commun. Heat Mass Transf.* **2022**, *137*, 106243. [[CrossRef](#)]
62. Rasool, G.; Shafiq, A.; Khan, I.; Baleanu, D.; Sooppy Nisar, K.; Shahzadi, G. Entropy Generation and Consequences of MHD in Darcy-Forchheimer Nanofluid Flow Bounded by Non-Linearly Stretching Surface. *Symmetry* **2020**, *12*, 652. [[CrossRef](#)]
63. Sajid, T.; Ayub, A.; Shah, S.Z.H.; Jamshed, W.; Eid, M.R.; el Din, E.S.M.T.; Irfan, R.; Hussain, S.M. Trace of Chemical Reactions Accompanied with Arrhenius Energy on Ternary Hybridity Nanofluid Past a Wedge. *Symmetry* **2022**, *14*, 1850. [[CrossRef](#)]
64. Sajid, T.; Jamshed, W.; Shahzad, F.; Ullah, I.; Ibrahim, R.W.; Eid, M.R.; Arshad, M.; Khalifa, H.A.E.; Alharbi, S.K.; el Din, M.E.S.T. Insightful into dynamics of magneto Reiner-Philippoff nanofluid flow induced by triple-diffusive convection with zero nanoparticle mass flux. *Ain Shams Eng. J.* **2022**, *6*, 101946. [[CrossRef](#)]
65. Jafar, A.B.; Shafie, S.; Ullah, I.; Safdar, R.; Jamshed, W.; Pasha, A.A.; Rahman, M.M.; Hussain, S.M.; Rehman, A.; el Din, E.S.M.T.; et al. Mixed Convection Flow of an Electrically Conducting Viscoelastic Fluid past a Vertical Nonlinearly Stretching Sheet. *Sci. Rep.* **2022**, *12*, 14679. [[CrossRef](#)]